

Optical characterization and manipulation of alkali metal nanoparticles in porous silica

A. Burchianti^{1,a}, A. Bogi¹, C. Marinelli¹, C. Maibohm^{1,2}, E. Mariotti¹, S. Sanguinetti³, and L. Moi¹

¹ CNISM and Physics Department, University of Siena, 53100 Siena, Italy

² Mads Clausen Institute, NanoSYD, University of Southern Denmark, 6400 Sønderborg, Denmark

³ Physics Department, University of Pisa, 56127 Pisa, Italy

Received 5 May 2008

Published online 22 August 2008 – © EDP Sciences, Società Italiana di Fisica, Springer-Verlag 2008

Abstract. Rubidium and cesium metal nanoparticles were grown in nanoporous silica samples placed in alkali vapor cells. Their size and shape were investigated by measuring the sample optical transmittance. Spectral changes due to photodesorption processes activated by weak light were also analyzed. Alkali atoms photoejected from the silica walls diffuse through and out of the nanopores, modifying both the nanoparticle distribution in the silica matrix and the atomic vapor pressure in the cell volume. The number of rubidium and cesium atoms burst out of the samples was measured as a function of photon energy and fluence. The optical absorption measurements together with the analysis of the photodesorption yield give a complete picture of the processes triggered by light inside the nanopores. We show that atomic photodesorption, upon proper choice of light frequency and intensity, induces either growth or evaporation of nanosized alkali metal clusters. Cluster size and shape are determined by the host-guest interaction.

PACS. 78.67.Bf Nanocrystals and nanoparticles – 68.43.Tj Photon stimulated desorption – 64.70.Nd Structural transitions in nanoscale materials

1 Introduction

The physical properties of metallic nanoparticles (NPs) greatly differ from those of the corresponding bulk material because of surface and quantum size effects. In particular, they exhibit tunable optical properties associated with their surface plasmon resonances, which are useful, for example, in the development of data storage media [1,2], optical switching [3,4], biophysical and chemical sensors [5–7]. In recent years, significant efforts have been made to produce controlled ensembles of NPs by methods ranging from photochemical reactions to metal vapor synthesis [8]. Independently of the used production technique, NPs need to be capped with protecting agents or embedded in solid matrices so that their agglomeration and precipitation are prevented. Among solid supports, mesoporous materials, due to their huge inner surface and small pore size, are particularly suitable to host metallic NPs, as confirmed by several experiments [9–14]. The most extensive investigation has been carried out with Ag and Au noble metal NPs. On the other hand, very little has been made with alkali metal NPs in porous media, except for the case of small clusters in zeolite crystals [15–17]. The lack of attention to alkali metals, although they have tunable plasmon resonances in the visible region as gold and

silver metal have, is due to their high chemical reactivity, which makes their exposure to air impossible. Nevertheless, despite this drawback, alkali metal NPs can be grown inside porous dielectric structures and can be easily controlled by light, opening perspectives for applications [18].

In this work nanoporous silica samples are inserted into sealed glass cells filled either with rubidium or cesium vapor. Alkali atoms flow from the cell volumes into the porous samples and are adsorbed on the silica walls causing formation of atomic layers and NPs; the latter are characterized in terms of their size and shape by means of optical transmission measurements. We found that the alkali metal phase equilibrium in the silica matrix is modified by light, which induces atomic detachment and diffusion through the nanopores. These effects move atoms from layers to NPs and vice versa, consequently producing a measurable change of the sample optical response. As previously observed for Rb atoms stored in porous silica [18,19], atomic photodesorption, depending on light frequency, occurs either at the silica walls or at the cluster surface. In the following we will refer to the first effect as light-induced atomic desorption [20,21], shortly LIAD, and to the second as surface-plasmon induced desorption [22], shortly SPID.

LIAD is a non-thermal desorption process observed with alkali atoms adsorbed on a wide variety of materials

^a e-mail: burchianti@unisi.it

like organic films [20,21,23–27], alkali metal films [28,29], Vycor [30], porous silica [31], sapphire [32] and stainless steel [33]. Nowadays LIAD is commonly used for efficient loading of magneto-optical traps [30,33,34], atom-chips [35] and photonic bandgap fibers [36]. A possible explanation of LIAD from SiO₂ has been given in terms of localized electronic excitation at the surface defects [37].

SPID has been reported for Na and K NPs supported on a crystal surface [38], for Rb clusters dipped into a film of liquid helium [39] or embedded in porous silica [19]. It is a non-thermal effect due to the excitation of surface plasmon oscillations, which produce atomic desorption from NPs. The desorption dependence on photon energy is determined by the dipolar surface plasmon excitation, which is responsible for the electric field enhancement at the cluster surface [38]. This process has been used to manipulate with laser light the size and shape distributions of metallic islands deposited on surfaces [40].

In our system it is possible to distinguish between the LIAD and SPID contribution to the atomic photodesorption. In fact, the surface plasmon resonances of Rb and Cs NPs embedded in porous silica are located in the red-NIR (near infrared) region, whereas the LIAD effect becomes significantly large in the green-blue spectral region. The light-induced phase transformations in the alkali metal loaded porous silica samples are investigated by recording the sample absorbance, from the infrared to the visible region, before and after irradiation. The photodesorption dependence on light frequency and intensity is studied by measuring the number of alkali atoms photoejected from the porous sample into the cell volume. The effects produced by light on NPs are directly related to the photodesorption processes by simultaneously monitoring, during illumination, the alkali vapor pressure in the cell volume and the sample transmission at a suitable fixed light frequency. From the experimental analysis, it comes out that in the silica matrix LIAD increases the atomic mobility of both Rb and Cs and that the photodetached atoms grow up metal clusters. On the other hand, optical radiation with frequency tuned to the surface plasmon resonances desorbs atoms from NPs, via SPID, and from the pore surface, via LIAD. This causes a competition between cluster evaporation and growth. We find that the result of this competition is different in Rb and Cs loaded porous silica. Furthermore, we show that the light-grown NPs, as well as the ones formed in the dark, exhibit well-defined surface plasmon resonances characteristic of the atomic species. This provides information on cluster size and shape distributions, which depend on the host-guest system.

2 Experiment

In this section we report the techniques used to prepare alkali metal loaded porous silica samples and the experimental procedures adopted for both optical analysis of alkali metal NPs and photodesorption measurements. The experimental set-up is sketched in Figure 1. Porous plates ($30 \times 15 \times 1$) mm³ made from borosilicate glass are placed

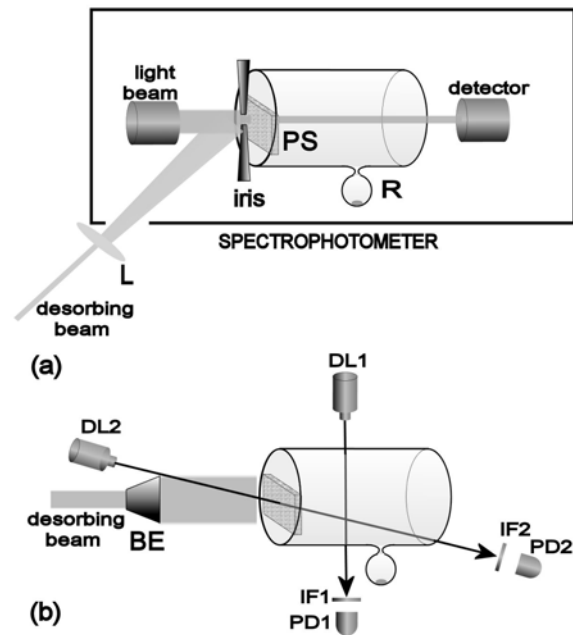


Fig. 1. Sketch of the experimental set-up. (a) PS: porous silica sample; R: alkali metal reservoir; L: lens. (b) DL1: alkali vapor probe laser; DL2: porous silica transmission probe laser; IF1, IF2: interference filters; PD1, PD2: photodiodes; BE: beam expander.

inside Pyrex alkali vapor cells. The samples have a random interconnected network of elongated pores with a mean pore diameter of 17 nm. The porosity is approximately 50% of the total glass volume and the sample inner surface is about 40 m² [41]. Samples are mechanically fixed close to one of the cell windows. Cells are prepared by connecting them for a few days to a vacuum system and by heating them to speed up impurity desorption. Before sealing them off, alkali metal is distilled in a side arm connected to the cell body through a short capillary; no buffer gas is added. Once closed, the cell is kept at room temperature in the dark and the sample is loaded with alkali atoms supplied by the reservoir. After a few days the alkali vapor density in the cell becomes stable and atomic desorption is observed when the sample is illuminated by ordinary or laser light.

We have tested several cells with different geometries filled either with Rb or Cs. Since the cells loaded with the same alkali metal show similar features, in the following we will make reference to two identical cylindrical Pyrex cells, 34 mm in diameter and 80 mm in length, one loaded with Rb and the other with Cs. This makes straight a direct comparison between Rb and Cs. In the cells containing a porous silica sample we have measured a vapor density lower than the saturated one. At room temperature, the atomic density in the Rb cell is about 30% of the saturated Rb vapor density (4.5×10^9 atoms/cm³ in Ref. [42]), whereas the measured density in the Cs cell is about 80% of the saturated Cs vapor density (3.0×10^{10} atoms/cm³ in Ref. [42]). Similar results are also reported in paraffin and siloxane coated alkali vapor cells [25,43]. This is due

to continuous absorption of atoms into the organic coating or adsorption at the glass surface.

The porous silica absorbance is obtained using a Varian Cary 5000 UV-Vis-NIR spectrophotometer (Fig. 1a). Once the cell has been inserted inside the instrument, the sample absorbance is recorded before and after sample illumination without removing the cell. This method allows us to evaluate the light-induced spectral change of the alkali metal-silica glasses avoiding spurious changes due to the cell realignment. The time evolution of both NPs and photodesorption yield are measured with a different experimental scheme (Fig. 1b). The Rb or Cs atomic density is detected by means of a weak probe beam resonant with either the Rb D2 line at 780 nm or the Cs D2 line at 852 nm. The probe laser is scanned across the Doppler spectrum of the Rb or Cs D2 transitions. The spectra are continuously acquired and then elaborated to extrapolate the vapor density. A probe beam, generated by a diode laser emitting in the red-NIR region, is used to measure the porous silica transmission. The desorbing light is provided by different sources covering a broad spectral range from the blue to the NIR region: argon-ion laser, cw doubled Nd:YAG laser, several diode lasers and a high-pressure Hg lamp.

3 Results and discussion

3.1 Size and shape of nanoparticles produced by atomic diffusion in the dark

As the porous samples are exposed to the alkali vapor present in the cells, their transparency changes. The absorbance of the Rb and Cs loaded porous silica samples together with the absorbance of a pure porous silica plate are respectively reported in Figures 2a and 2b. The doped samples show broad absorption bands in the red-infrared region, which are due to surface plasmon resonances of metal NPs grown in the silica pores. Their peak frequencies and widths are determined by several parameters such as cluster size and shape distributions, intrinsic size effects, interactions with the surrounding medium and with neighbor clusters [44]. The narrow peaks present in all spectra are due to the glass absorption.

Both alkali metal loaded silica glasses present two separated plasmon bands ((1) and (2) in Figs. 2a and 2b). In the Rb loaded sample the band (1) splits into two close peaks located around 1.5 eV. The band (2) occurs at about 0.8 eV. In the Cs loaded sample the band (1) is observed around 1.2 eV. The band (2) falls in the infrared and it cannot be completely resolved because it partially overlaps the silica absorption band. The Rb surface plasmon bands are blue shifted with respect to the Cs ones, in agreement with the bulk plasma frequencies of the two alkali metals [45]. For both samples the bands at higher energies are due to the formation of spheroidal metallic clusters. These particles have a size of a few nanometers because of the pore confinement. In order to provide an estimation of the extinction cross-section of alkali metal NPs in porous

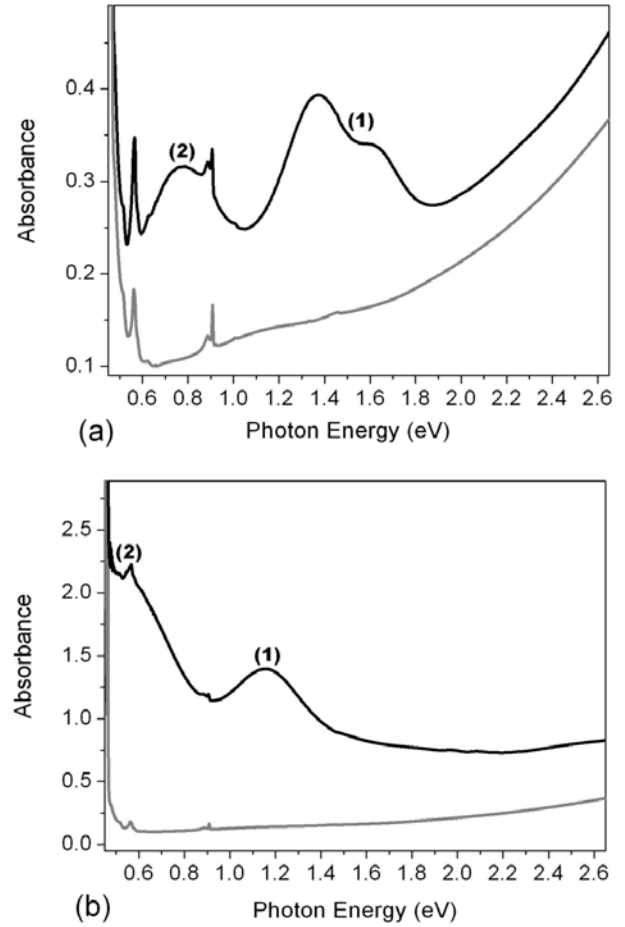


Fig. 2. (a) Optical spectra of Rb doped (black curve) and pure (gray curve) porous silica. (b) Optical spectra of Cs doped (black curve) and pure (gray curve) porous silica.

silica, we apply Gans theory [46] that describes the optical properties of randomly oriented spheroids with size $R \ll \lambda$. The extinction cross-section σ_{ext} is given by the equation [47]:

$$\sigma_{ext}(\omega) = V \frac{\omega}{3c} \epsilon_m^{3/2} \sum_i \frac{\epsilon_2(\omega) (1/P_i^2)}{\epsilon_2(\omega)^2 + \left(\epsilon_1(\omega) + \epsilon_m \frac{1-P_i}{P_i} \right)^2}, \quad (1)$$

where V is the particle volume, ω is the frequency of the incident light, ϵ_m is the dielectric constant of the embedding medium and $\epsilon_1(\omega)$ and $\epsilon_2(\omega)$ are respectively the real and imaginary part of the metal dielectric function. The terms P_i represent the depolarising factors for the symmetry axes a , b and c of the spheroid. For pancake-shaped spheroids ($c < a = b$) the depolarising factors are defined as [48]:

$$P_c = \frac{1+e^2}{e^3} (e - \tan^{-1} e), \quad (2)$$

$$P_a = P_b = \frac{1}{2} (1 - P_c), \quad (3)$$

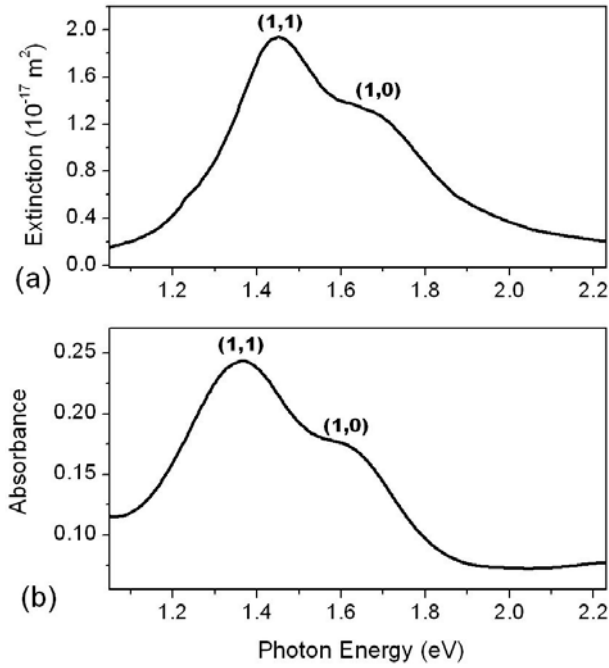


Fig. 3. (a) Calculated extinction cross-section of Rb oblates in porous silica. The medium dielectric constant is 2.25, the mean radius is 3 nm and the aspect ratio is 0.8. (b) Difference between the measured absorbance of Rb doped and pure porous silica.

with

$$e = \sqrt{\frac{a^2}{c^2} - 1}. \quad (4)$$

The ratio between the short and long semiaxes c/a is known as the particle aspect ratio. We use the dielectric constants of Rb and Cs measured by Smith [49] and we modify them according to reference [50] in order to take into account the damping effects due to the small particle size. For metallic particles partially embedded in a silica matrix the cluster-surrounding interactions are rather difficult to describe because the symmetry of the medium is broken. Nevertheless the system can be schematized by supposing the NPs implanted in a medium with a relative dielectric constant ϵ_m between 1 (vacuum) and 2.25 (glass). These limit values are respectively obtained in the case of free and fully embedded clusters. Although the exact value of ϵ_m is unknown, its main effect on the surface plasmon resonance is to shift its frequency without changing its shape. An overestimation of ϵ_m causes a red shift of the resonance, while an underestimation a blue shift. We take as free parameters the mean particle radius R , the aspect ratio c/a and we vary ϵ_m between 1 and 2.25. A qualitative agreement between model and data is achieved using the following values: $\epsilon_m = 2.25$, $R = 3$ nm for both Rb and Cs, $c/a = 0.8$ and 0.9 for Rb and Cs respectively. The calculated extinction cross-sections are shown in Figures 3a and 4a for Rb and Cs respectively. For comparison the corresponding measured absorbance spectra are reported in Figures 3b and 4b after subtraction of the contribution of the pure silica sample.

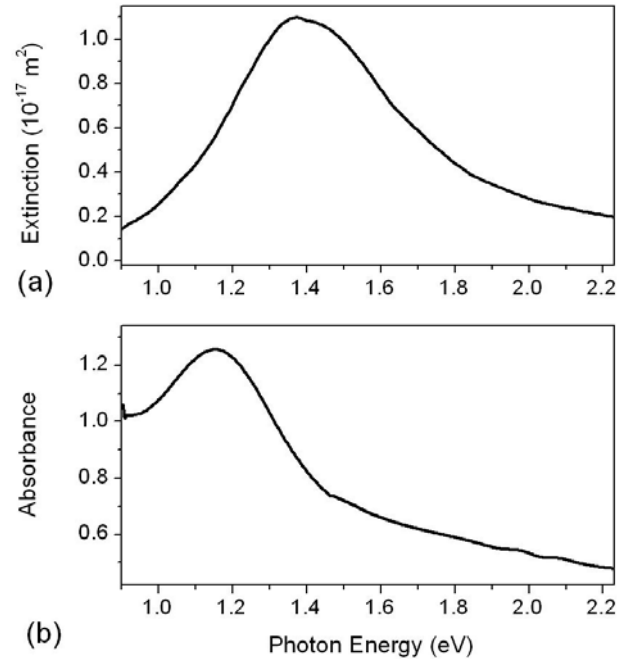


Fig. 4. (a) Calculated extinction cross-section of Cs oblates in porous silica. The medium dielectric constant is 2.25, the mean radius is 3 nm and the aspect ratio is 0.9. (b) Difference between the measured absorbance of Cs doped and pure porous silica.

The shapes of the plasmon resonances predicted by the model are in good agreement with the observed ones. This means that in both doped samples the bands at higher energies ((1) in Figs. 2a and 2b) are associated with a narrow distribution of quasi-spherical NPs. The estimated particle size is further confirmed by the fact that we observe similar spectra in porous silica samples with mean pore diameter of 7 and 4 nm. As it follows from the evaluated aspect ratios, the Rb spheroids are slightly less spherical than the Cs ones. Therefore the Rb surface plasmon resonance splits into two modes denoted in Figures 3a and 3b as (1,0) and (1,1). The mode (1,0) at higher frequency is due to the collective electron oscillations along the particle short axes. The mode (1,1) at lower frequency is produced by the plasmon excitation along the long axes. The plasmon peak associated with the degenerate mode (1,1) is higher than the peak associated with the nondegenerate mode (1,0). Although the shapes of the measured plasmon bands are consistent with the calculated ones, their resonance frequencies show a significant red shift. This shift cannot be corrected by increasing ϵ_m more because it is already at the maximum value. The effect is more pronounced in the Cs than in the Rb loaded silica sample. This discrepancy can be attributed to the fact that the model roughly describes the cluster-surrounding interactions and neglects the cluster-cluster interactions. Indeed equation (1) is valid only for a system of well-isolated non-interacting particles. As the cluster concentration in the sample increases, the distance between particles becomes comparable with their size and the plasmon resonance shifts to lower frequencies [44]. Therefore it is possible

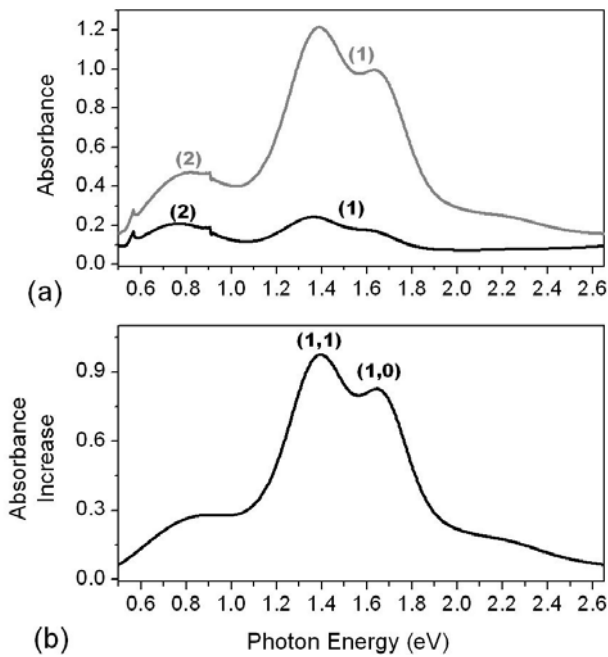


Fig. 5. (a) Optical spectra of Rb doped porous silica before (black curve) and immediately after illumination (gray curve) with a Hg lamp. Spectra are presented after subtraction of the absorbance of pure porous silica. (b) Light-induced absorbance increase of Rb doped porous silica.

that in our system the red shift is in part produced by the interaction between neighbor clusters.

We have still to explain the absorption band in the infrared ((2) in Figs. 2a and 2b) observed for both alkali metal loaded samples. According to our analysis, it is related to pore regions where the metal concentration is so high that the interparticle distance becomes smaller than the particle size. Therefore local aggregation occurs causing the presence of an additional plasmon band at lower frequency [44]. The existence of sample regions at higher metallic concentration can be correlated with the filling of the smaller silica pores. From the absorption spectra it follows that in the sample loaded with Rb the fraction of large aggregates is smaller than in the one loaded with Cs. This means that the Rb filling factor is lower than the Cs one in agreement with the alkali vapor pressures measured in the cell bodies.

3.2 Nanoparticle growth induced by desorbing light

As light hits the porous sample, the equilibrium inside the nanopores between NPs, atomic layers and vapor phase, is suddenly shifted. In this section, we present measurements of the effects produced by UV-visible light on nanoparticle spectra.

Upon UV-visible irradiation, the surface plasmon band intensity increases. In Figure 5a the absorbance of the Rb loaded silica sample at equilibrium in the dark is compared with the one recorded immediately after exposure to a high-pressure Hg lamp. Both signals are presented af-

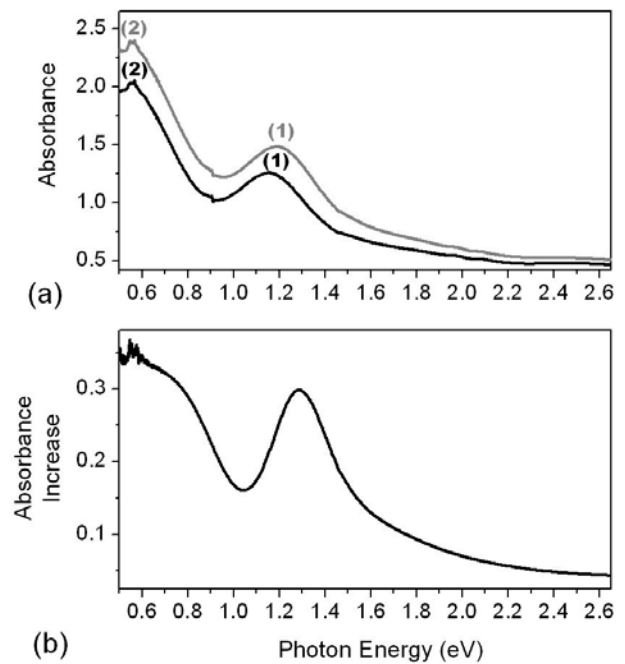


Fig. 6. (a) Optical spectra of Cs doped porous silica before (black curve) and immediately after illumination (gray curve) with an Hg lamp. Spectra are presented after subtraction of the absorbance of pure porous silica. (b) Light-induced absorbance increase of Cs doped porous silica.

ter subtraction of the absorbance of the pure porous silica sample. In order to make the light-induced spectral change more clear, we give in Figure 5b the difference between the sample absorbance after and before illumination. The light intensity is 10 mW/cm^2 and the illumination time is two minutes. The corresponding measurements for the Cs loaded silica sample are shown in Figures 6a and 6b. Results similar to the ones reported here are also found by using monochromatic green or blue light [19]. In both alkali metal-silica glasses, light causes an intensity increase of the surface plasmon band at higher frequency ((1) in Figs. 5a and 6a) that we attributed to quasi-spherical alkali metal NPs. This result could be due to the formation of new clusters as well as by the growth in size of the existing clusters. As the bands are not significantly changed, we deduce that the particles formed or modified by light are similar in size and shape to the ones present at the equilibrium. Moreover, we note that in both alkali metal-silica glasses the peaks are blue shifted so that their resonance frequencies are closer to those predicted by the theory. This can be explained by assuming that light builds up new isolated clusters on the pore walls. Therefore the new NPs are preferentially formed in the partially empty regions of the silica bulk.

In the Rb doped porous silica sample the mode (1,0) increases with respect to the mode (1,1) (compare Fig. 5b with Fig. 3b). Nevertheless the distance between the two modes does not change showing that the particle aspect ratio remains close to one. Hence, in addition to quasi-spherical oblates, which are the dominant particle

distribution in the dark, light grows quasi-spherical cigar-shaped particles ($a > b = c$). Indeed for prolate particles, differently from oblate ones, the modes (1,0) and (1,1) are respectively degenerate and nondegenerate, as a consequence the plasmon peak at higher frequency is higher than the one at lower frequency. In the Cs doped porous silica sample the plasmon band produced by the light-grown Cs spheroids is better resolved from the background absorption (compare Fig. 6b with Figs. 4b and 2b). This is due to the fact that at equilibrium in the dark this band partially overlaps the band at lower energy, which has a smaller relative increase with illumination.

In both alkali metal-silica glasses the intensity increase of the surface plasmon band in the infrared region ((2) in Figs. 5a and 6a) shows that light also causes formation of metallic aggregates. This is a weaker effect in the Rb-silica glass, supporting the hypothesis that the production of quasi-spherical dispersed Rb NPs prevails. On the contrary, it is significant in the Cs-silica sample. In addition, the equilibrium absorbance of the Cs-silica glass is remarkably higher than the one of the Rb-silica glass. Nevertheless its increase due to illumination is lower. These results suggest that the free volume in the porous silica sample filled with Rb is considerably larger than in the one filled with Cs. This fact makes the formation of separated Rb NPs in the porous matrix possible.

The photoinduced phase transformations of Rb and Cs inside the nanopores are reversible. Once the light is switched off, the light-grown clusters evaporate, with a characteristic time ranging from few to several hours, to restore the equilibrium condition. As a result the surface plasmon band intensity slowly decreases to the initial value.

3.3 Photodesorption yield measurements

In order to get more insights on the role of photodesorption processes in the light-induced changes of alkali metal NPs, we measure, during a light on-off cycle, the variation in the cell volume of the atomic density $\Delta n(t) = n(t) - n_0$, with respect to the equilibrium value n_0 .

The amount of desorbed atoms that diffuse out of the porous silica sample depends on several parameters, such as illumination time, light frequency, atomic distribution in the matrix, transport mechanisms through the nanopores and relaxation of the vapor density to the equilibrium value. Although $\Delta n(t)$ can be used to study the desorption dynamics, it is more convenient to introduce another parameter to provide an estimation of the desorbing efficiency [31]. We define the relative increasing rate R_n of the vapor density, immediately after the desorbing light is switched on at $t = t_L$, as follows:

$$R_n = \frac{1}{n_0} \left(\frac{dn}{dt} \right)_{t=t_L}. \quad (5)$$

The desorbing rate R_n defined in this way is mainly due to the atoms desorbed from the pores that are close to the outer sample surface. In Figures 7a and 7b plots of R_n

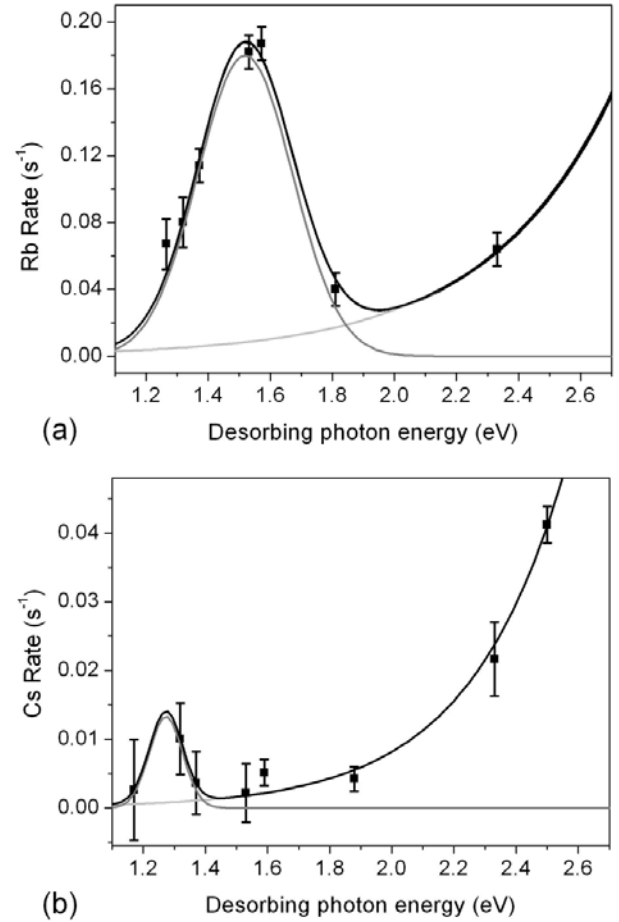


Fig. 7. (a) Rb and (b) Cs rates as a function of desorbing photon energy. The light intensity is 2 mW/cm². Black curves are the sum of two functions: an exponential one and a Gaussian one, which describe LIAD and SPID respectively.

versus desorbing photon energy are given for the porous silica samples filled with Rb and Cs respectively. The light intensity is fixed to 2 mW/cm² for all frequencies and both samples are completely illuminated. As previously observed for Rb loaded porous silica [19], R_n shows a monotonic increase with the photon energy, due to LIAD, and a pronounced broad peak in the red-NIR region, due to SPID. The photon energies, corresponding to the peak maxima, are different for the two alkali atoms. They are about 1.5 eV and 1.3 eV for Rb and Cs respectively.

While all clusters dispersed in the bulk matrix contribute to the absorbance spectra, the desorbing rate R_n mainly depends on atomic layers and on NPs close to the interface with the cell vapor phase. Keeping in mind this difference, we compare the desorbing rate dependence on photon energy with the spectra of the two alkali metal loaded samples. For the Rb loaded sample the maximum of desorbing efficiency falls in the first plasmon band occurring in the spectrum ((1) in Fig. 2a). For the Cs loaded sample the peak of desorbing band is on the blue edge of the first plasmon band at higher energy ((1) in Fig. 2b). These results give direct evidence that red-NIR light desorbs atoms from spheroidal NPs.

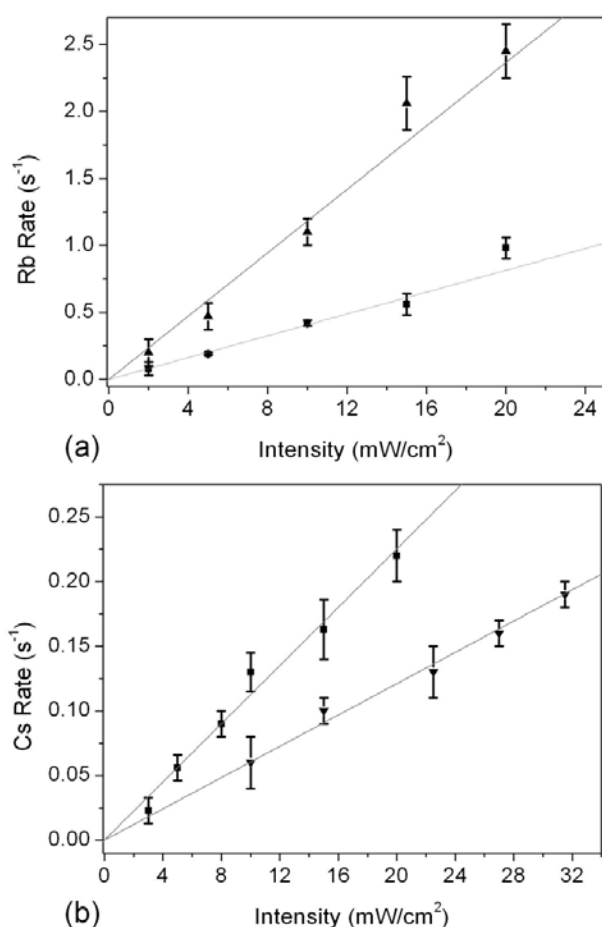


Fig. 8. (a) Rb rate as a function of laser light intensity for two values of photon energy: 1.53 eV (up triangles) and 2.33 eV (squares). (b) Cs rate as a function of laser light intensity for two values of the photon energy: 1.32 eV (down triangles) and 2.33 eV (squares).

In Figures 8a and 8b the rates of the Rb and Cs doped silica glasses as a function of light intensity are shown when the whole samples are illuminated. In both cases the rate dependence is given for two photon energies, selected to excite either one photodesorption process or the other. For both atoms the photon energy associated with LIAD is 2.33 eV, whereas the photon energies associated with surface plasmon oscillations are 1.53 eV and 1.32 eV for the Rb and Cs-silica glasses respectively. These last values are close to the maximum efficiency of photodesorption from clusters. In all cases the desorbing rate increases linearly with the number of incident photons. This is a clear indication that desorption is not triggered by thermal effects. Moreover, it is worth noting that photodesorption from clusters and from pore surface is observed with extremely low light intensities; no intensity threshold can be extrapolated. Although atomic desorption is due to non thermal mechanisms of excitations, we have to take into account that, in the case of resonant absorption of light by NPs, the particle temperature rises as the laser fluence increases. Therefore at higher intensities both thermal and non-thermal desorption occur at the cluster surface.

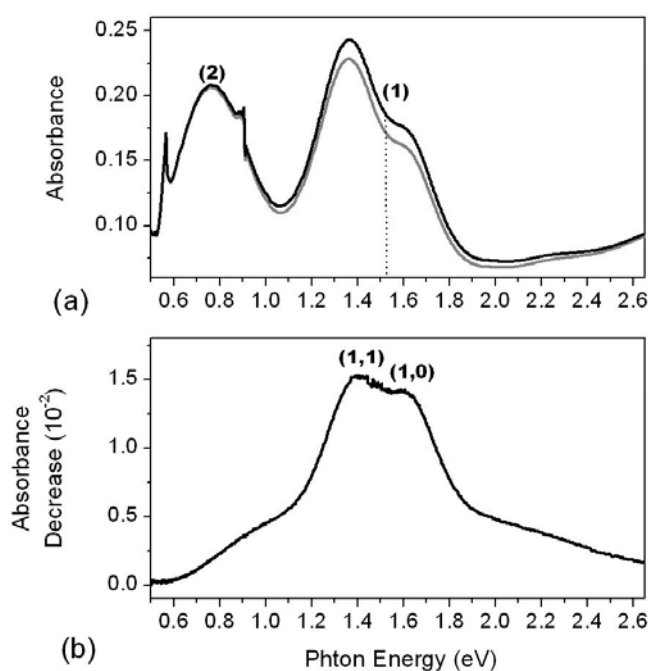


Fig. 9. (a) Optical spectra of Rb doped porous silica before illumination (black curve) and immediately after illumination (gray curve) at 1.53 eV. Spectra are presented after subtraction of the absorbance of pure porous silica. The dot vertical line indicates the position of the laser frequency. (b) Absorbance decrease of Rb doped porous silica induced by light at 1.53 eV.

The photodesorption measurements prove that the mechanism of light-induced cluster growth is correlated to LIAD. UV-visible photons induce atomic photodesorption from the pore surface. A small part of the desorbed atoms diffuses out of the sample and increases the alkali vapor pressure inside the cell body, while the others, trapped in the matrix, recondense on the pore walls forming clusters. In the dark, the adsorbed atoms move back from clusters to layers.

3.4 Competition between light-induced nanoparticle growth and evaporation

The desorbing rate dependence on photon energy shows that NIR light desorbs atoms both from layers and clusters. Therefore, cluster formation via LIAD, as well as cluster evaporation via SPID, can be induced by the same photon frequency. Figure 9a shows the absorbance of the Rb loaded sample before and immediately after exposure to light at 1.53 eV. Both spectra are presented after subtraction of the absorbance of the pure porous silica sample. Figure 9b gives the difference between the sample absorbance before and after illumination. The laser intensity is 180 mW/cm² and the illumination time is two minutes. The absorbance falls over a broad frequency range with a maximum variation around the laser frequency. Although the absorbance decrease due to cluster evaporation is considerably smaller than its increase produced by

cluster growth, the relative spectral change is similar in both cases. Indeed, also NIR light mainly modifies the Rb plasmon band at higher frequency ((1) in Fig. 2a). This happens now because the light frequency matches the surface plasmon resonance of quasi-spherical Rb NPs, consequently atomic photodesorption takes place from their surface. The ratio between the mode (1,1) and the mode (1,0) increases (compare Fig. 9b with Fig. 3b), showing that cigar-shaped particles are preferentially evaporated. This could be a consequence of the fact that prolate particles are less stable than oblate ones. As proof of this, we recall that only a small fraction of the Rb spheroids formed at equilibrium in the dark are prolate. Moreover, we observe that the light-burned “hole” in the spectrum spreads from the infrared to the visible region. In fact, although the main effect produced by NIR light is to evaporate separated Rb spheroids, also interacting cluster systems are destroyed. This is due to the fact that aggregates such as linear chains have the transverse excitation mode, which overlaps the plasmon band produced by separated spheroids.

The Cs loaded porous silica sample has a different behavior as compared to the Rb loaded one. In fact, when the sample is illuminated with resonant NIR light at 1.17 eV (laser intensity: 180 mW/cm², illumination time: 2 min) cluster growth is observed as in the case of UV-visible illumination. Therefore, in the Cs-silica glass the cluster formation rate due to LIAD is higher than the evaporation rate due to SPID.

Other differences between Rb and Cs loaded porous silica are put in evidence by monitoring the temporal evolution of both desorbed atoms in the cell volume and NPs, when the samples are exposed to a sequence of green-NIR light pulses. In Figure 10a the sample transmission at 1.58 eV and the variation of the atomic density Δn are shown when the Rb loaded sample is successively illuminated by green light at 2.33 eV and NIR light at 1.53 eV. The illumination time is 100 s for both light pulses and the dark time between them is 500 s. The green and NIR laser powers are 10 mW and 240 mW respectively. The sample area illuminated by the NIR light (10 mm²) is inside the one illuminated by the green light (30 mm²). As shown in Figure 10a, during the green light pulse the sample transmission decreases, because atoms photodetached from the silica surface build up clusters. On the contrary, during the NIR pulse, the sample transmission rises as a consequence of cluster evaporation. During both light pulses, a small fraction of photodetached atoms diffuse out of the sample and increases the atomic density inside the cell. In the dark the formed clusters dissolve and the sample transmission recovers.

The corresponding measurement made with the Cs-silica glass is reported in Figure 10b. In this case both green and NIR light decrease the sample transmission via cluster formation, while the Cs vapor pressure inside the cell increases for both light frequencies. We note that, during the NIR light pulse, Cs clusters start to evaporate probably in consequence of an increase of the particle temperature. In support of this interpretation, we observe

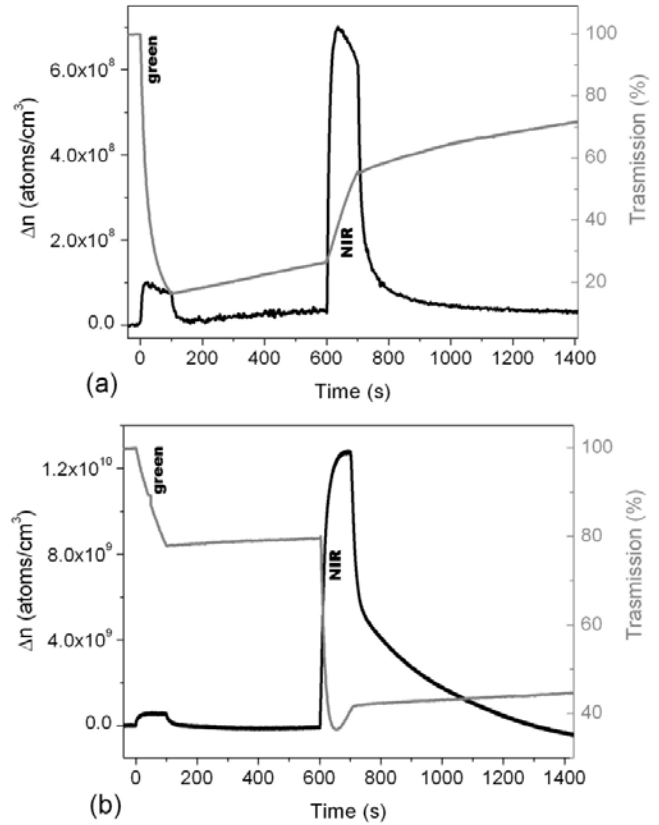


Fig. 10. (a) Rb and (b) Cs doped porous silica exposed to a sequence of green-NIR light pulses. The laser powers are 10 mW and 240 mW and the illuminated areas are 30 mm² and 10 mm² for green (2.33 eV) and NIR (1.53 eV) light respectively. Black curves give the alkali atom vapor density variation inside the cell and gray curves the glass transmission at 1.58 eV.

that at lower laser intensities cluster evaporation does not occur. Moreover the dynamics of the Cs vapor phase, after the light is switched off, is characterized by two relaxation times. The presence of the longer one shows that a thermal process has been activated. Also in this case, when the light is turned off, the transmission variation is stopped. Then the system relaxes to the equilibrium condition with a recovery time considerably slower than the one observed for the Rb-silica glass. The faster decay of the light-grown Rb clusters could be related to their shape. As shown in Section 3.2, whereas the light-grown Cs particles are similar to those formed in the dark, the Rb ones have a slightly different symmetry. Indeed light increases the ratio between Rb prolates and oblates with respect to equilibrium in the dark. The outcome is a high fraction of unstable particles, which evaporate more easily.

4 Summary and conclusions

Our experiments show that alkali metal clusters grown in porous silica by vapor diffusion have well defined size and shape. This effect is due to the interaction with the porous

matrix, which favors formation of Rb and Cs nanosized quasi-spherical particles. Together with separated alkali metal spheroids, cluster aggregates are also formed on the silica walls. The presence of interacting cluster systems is correlated with the alkali metal filling factor. Cluster aggregation occurs preferentially in Cs than in Rb loaded porous silica, because the Cs vapor pressure at room temperature is about one order of magnitude higher than the Rb one.

Illuminating alkali metal loaded porous silica with UV-visible light causes further growth of NPs. This result relies on the LIAD effect. Light induces atomic detachment from the pore walls and increases atomic diffusion in the porous network. Desorbed atoms flow through the matrix until they remain trapped at surface defects, which act as nucleation sites for cluster growth. As a consequence atoms shift from layers to clusters. The experimental analysis points out that NPs formed by light have roughly the same size and shape as clusters produced by atomic diffusion in the dark. Such a result confirms that the confinement geometry is determinant for the structural properties of existing particles. In Rb loaded porous silica the dominant effect produced by radiation is the formation of separated spheroids, whereas in Cs loaded porous silica it is comparable with the creation of larger metallic aggregates.

When the desorbing light matches the alkali metal surface plasmon resonances, it produces electronic oscillations at the cluster surface. As a consequence atomic desorption takes place from NPs. Atoms desorbed via SPID condense on the inner silica surface forming either layers or clusters. In the latter case, they are again evaporated by resonant light until they move to the pore surface. This mechanism increases the atomic concentration in layers against the cluster density. Nevertheless, due to LIAD, which is simultaneously present with SPID, atomic layers are destroyed. This produces antagonism between layers and clusters. We find that cluster evaporation is dominant in Rb loaded porous silica, whereas cluster growth prevails in Cs loaded porous silica.

The alkali metal concentration could play a role in the different behavior between Rb and Cs also in the case of NIR light. Indeed the amount of adsorbed atoms changes the cluster aggregation state and consequently modifies the light-assisted diffusion of atoms inside the matrix. At the current stage further experiments are required to fully characterized the dependence of cluster growth and evaporation on metal filling factor.

We note in conclusion that the work presented in this paper sheds new light on atomic photodesorption processes and their possible applications when nanostructures are involved.

We would like to thank M. Badalassi for cell manufacturing and the technical staff of the Physics Department of Siena for their continuous help. C. Maibohm acknowledges the financial support provided through the European Community's Human Potential Program undercontract HPRN-CT-2002-00304, FASTNet.

References

1. H. Ditlbacher, B. Lamprecht, A. Leitner, F.R. Aussenegg, *Opt. Lett.* **25**, 563 (2000)
2. J.W.M. Chon, C. Bullen, P. Zijlstra, M. Gu, *Adv. Funct. Mater.* **17**, 875 (2007)
3. M. Rini, A. Cavalleri, R.W. Schoenlein, R. López, L.C. Feldman, J.R.F. Haglund, L.A. Boatner, T.E. Haynes, *Opt. Lett.* **30**, 558 (2005)
4. Y. Takeda, O. Plaksin, J. Lu, N. Kishimoto, *Nucl. Instrum. Meth. B* **242**, 194 (2006)
5. T. Schalkammer, *Chem. Mon.* **129**, 1067 (1998)
6. D.A. Schultz, *Curr. Opin. Biotechnol.* **14**, 13 (2003)
7. A.D. McFarland, R.P. Van Duyne, *Nano Lett.* **3**, 1057 (2003)
8. *Clusters and Colloids. From Theory to Application*, edited by G. Schmid (VCH, Weinheim, Germany, 1994)
9. S.I. Lee, T.W. Noh, J.R. Gaines, Y.H. Ko, E.R. Kreidler, *Phys. Rev. B* **37**, 2918 (1988)
10. C.A. Foss, G.L. Hornyak, J.A. Stockert, C.R. Martin, *J. Phys. Chem.* **98**, 2963 (1994)
11. W. Cai, M. Tan, G. Wang, L. Zhang, *Appl. Phys. Lett.* **69**, 2980 (1996)
12. W. Cai, H. Hofmeister, T. Rainer, *Physica E* **11**, 339 (2001)
13. W. Chen, W. Cai, L. Zhang, G. Wang, L. Zhang, *Physica E* **238**, 291 (2001)
14. K.B. Ameen, T. Rajasekharan, M. Rajasekharan, *J. Non Cryst. Solids* **352**, 737 (2006)
15. Y. Nozue, T. Kodaira, T. Goto, *Phys. Rev. Lett.* **68**, 3789 (1992)
16. V.I. Srdanov, G.D. Stucky, E. Lippmaa, G. Engelhardt, *Phys. Rev. Lett.* **80**, 2449 (1998)
17. T. Nakano, K. Goto, I. Watanabe, F.L. Pratt, Y. Ikemoto, Y. Nozue, *Physica B* **374**, 21 (2006)
18. A. Burchianti, A. Bogi, C. Marinelli, E. Mariotti, L. Moi, *Opt. Express* **16**, 1377 (2008)
19. A. Burchianti, A. Bogi, C. Marinelli, C. Maibohm, E. Mariotti, L. Moi, *Phys. Rev. Lett.* **97**, 157404 (2006)
20. A. Gozzini, F. Mango, J.H. Xu, G. Alzetta, F. Maccarrone, R.A. Bernheim, *Nuovo Cim. D* **15**, 709 (1993)
21. M. Meucci, E. Mariotti, P. Bicchi, C. Marinelli, L. Moi, *Europhys. Lett.* **25**, 639 (1994)
22. W. Hoheisel, K. Jungmann, M. Vollmer, R. Weidenauer, F. Träger, *Phys. Rev. Lett.* **60**, 1649 (1988)
23. S.N. Atutov, V. Biancalana, P. Bicchi, C. Marinelli, E. Mariotti, M. Meucci, A. Nagel, K.A. Nasyrov, S. Rachini, L. Moi, *Phys. Rev. A* **60**, 4693 (1999)
24. C. Marinelli, A. Burchianti, A. Bogi, F. della Valle, G. Bevilacqua, E. Mariotti, S. Veronesi, L. Moi, *Eur. Phys. J. D* **37**, 319 (2006)
25. E.B. Alexandrov, M.V. Balabas, D. Budker, D. English, D.F. Kimball, C.H. Li, V.V. Yashchuk, *Phys. Rev. A* **66**, 042903 (2002)
26. A. Cappello, C. de Mauro, A. Bogi, A. Burchianti, S.D. Renzone, A. Khanbekyan, C. Marinelli, E. Mariotti, L. Tomassetti, L. Moi, *J. Chem. Phys.* **127**, 044706 (2007)
27. S. Gozzini, A. Lucchesini, L. Marmugi, G. Postorino, *Eur. Phys. J. D* **47**, 1 (2008)

28. J. Viereck, F. Stietz, M. Stuke, T. Wenzel, F. Träger, *Surf. Sci.* **383**, L749 (1997)
29. J. Brewer, H.G. Rubahn, *Chem. Phys.* **303**, 1 (2004)
30. C. Klempt, T. van Zoest, T. Henninger, O. Topic, E. Rasel, W. Ertmer, J. Arlt, *Phys. Rev. A* **73**, 013410 (2006)
31. A. Burchianti et al., *Europhys. Lett.* **67**, 983 (2004)
32. A.M. Bonch-Bruевич, T.A. Vartanyan, Y.N. Maksimov, S.G. Przhibel'ski, V.V. Khromov, *Zh. Eksp. Teor. Fiz.* **97**, 1077 (1990)
33. B.P. Anderson, M.A. Kasevich, *Phys. Rev. A* **63**, 023404 (2001)
34. S.N. Atutov et al., *Phys. Rev. A* **67**, 053401 (2003)
35. S. Du, M.B. Squires, Y. Imai, L. Czaia, R.A. Saravanan, V. Bright, J. Reichel, T.W. Hänsch, D.Z. Anderson, *Phys. Rev. A* **70**, 053606 (2004)
36. S. Ghosh, A.R. Bhagwat, C.K. Renshaw, S. Goh, A.L. Gaeta, B.J. Kirby, *Phys. Rev. Lett.* **97**, 023603 (2006)
37. D. Domínguez-Ariza, N. Lopez, F. Illas, G. Pacchioni, T.E. Madey, *Phys. Rev. B* **69**, 075405 (2004)
38. W. Hoheisel, M. Vollmer, F. Träger, *Phys. Rev. B* **48**, 17463 (1993)
39. A. Hatakeyama, K. Enomoto, N. Sugimoto, T. Yabuzaki, *Phys. Rev. A* **65**, 022904 (2002)
40. M. Vollmer, R. Weidenauer, W. Hoheisel, U. Schulte, F. Träger, *Phys. Rev. B* **40**, 12509 (1989)
41. I.M. Belusova, E.A. Gavronskaya, V.A. Grigor'ev, A.G. Skobelev, O.V. Andreeva, I.E. Obyknovennaya, A.S. Cherkasov, *J. Opt. Technol.* **68**, 882 (2001), porous glass samples were provided by I.E. Obyknovennaya
42. A.I.K. Kikoin, ed., *Tablitsi Fizicheskikh Velichin (Tables of Physical Values)* (Atomizdat, Moscow, 1976), cited by Ref. [24]
43. M.A. Bouchiat, J. Brosset, *Phys. Rev.* **147**, 41 (1966)
44. U. Kreibitz, M. Vollmer, *Optical Properties of Metal Clusters*, Vol. 25 of Springer Series in Materials Science (Springer, Berlin, 1995)
45. H. Raether, *Excitations of Plasmons and Interband Transitions by Electrons*, Vol. 88 of Springer Tracts in Modern Physics (Springer, New York, 1980)
46. R. Gans, *Ann. Phys.* **47**, 270 (1915)
47. S. Link, M. Mohamed, M. El-Sayed, *J. Phys. Chem. B* **103**, 3073 (1999)
48. C. Noguez, *J. Phys. Chem. C* **111**, 3806 (2007)
49. N.V. Smith, *Phys. Rev. B* **2**, 2840 (1970)
50. V.M. Rentería, J. García-Macedo, *Mat. Chem. Phys.* **91**, 88 (2005)